VIP Fluorescence Imaging Very Important Paper

Deutsche Ausgabe: DOI: 10.1002/ange.201511148
Internationale Ausgabe: DOI: 10.1002/anie.201511148

Noninvasive Staging of Kidney Dysfunction Enabled by Renal-Clearable Luminescent Gold Nanoparticles

*Mengxiao Yu, Jiancheng Zhou, Bujie Du, Xuhui Ning, Craig Authement, Leah Gandee, Payal Kapur, Jer-Tsong Hsieh, and Jie Zheng**

Abstract: *As a "silent killer", kidney disease is often hardly detected at an early stage but can cause lethal kidney failure later on. Thus, a preclinical imaging technique that can readily differentiate between the stages of kidney dysfunction is highly desired for improving our fundamental understanding of kidney disease progression. Herein, we report that in vivo fluorescence imaging, enabled by renal-clearable near-infrared-emitting gold nanoparticles, can noninvasively detect kidney dysfunction, report on the dysfunctional stages, and even reveal adaptive function in a mouse model of unilateral obstructive nephropathy, which cannot be diagnosed with routine kidney function markers. These results demonstrate that low-cost fluorescence kidney functional imaging is highly sensitive and useful for the longitudinal, noninvasive monitoring of kidney dysfunction progression in preclinical research.*

Nearly 10% of all adults worldwide suffer from a variety of kidney diseases that are often silent at an early stage, but can cause kidney failure later on.[1] Whereas various markers, such as blood urea nitrogen and creatinine, have been routinely used for staging kidney dysfunction, owing to the high functional preservation of the kidney, these markers are often insensitive to early-stage kidney dysfunction and remain within the normal range even when 65–75% of the normal kidney function has already been lost.[1a] To address this challenge, noninvasive in vivo imaging techniques, such as single-photon emission computed tomography (SPECT), magnetic resonance imaging, and computed tomography, have been widely used to assess the various stages of kidney dysfunction by real-time monitoring of the kidney clearance kinetics (KCK) of renal-clearable probes.[2] However, owing to their high cost, low accessibility, and the potential risk of exposure to radiation,[3] our fundamental understanding of kidney diseases in preclinical research has hardly been improved.

In vivo near-infrared fluorescence imaging is an inexpensive, highly sensitive, and widely used preclinical method for studying many diseases such as cancer.[4] However, the noninvasive fluorescence imaging of kidney dysfunction and its various stages has been a long-term challenge[5] owing to low kidney-contrast enhancement and the long-term nonspecific accumulation of organic dyes in background tissues.[6] To address these long-standing challenges, we recently applied renal-clearable near-infrared-emitting glutathione-coated gold nanoparticles (GS-AuNPs) as contrast agents for the fluorescence imaging of KCK in normal mice.[6] We were able to noninvasively monitor the KCK with a 50-fold increase in the kidney-contrast enhancement compared to that obtained with conventional organic dyes. However, the fundamental question of whether such fluorescence imaging techniques based on the use of GS-AuNPs are sensitive enough to noninvasively differentiate between various kidney dysfunction stages is still unanswered, but it is key to the future success of fluorescence imaging as a widely accessible preclinical method for studying kidney function.

For our studies, a unilateral ureteral obstruction (UUO) mouse model, a well-established preclinical model for ureteropelvic junction obstruction, which is asymptomatic at an early stage but can cause renal failure if not treated promptly in newborns,[5,7] was used. We found that the time fluorescence intensity curves (TFICs) derived from the kidney clearance of the renal-clearable near-infrared-emitting GS-AuNPs were extremely sensitive to kidney function impairments that were hardly detected with the kidney function markers blood urea nitrogen and serum creatinine (Supporting Information, Table S1). We not only directly identified kidneys with impaired function (reduced blood perfusion and decreased clearance) but could also differentiate between dysfunction stages (mild vs. severe dysfunction). These results were consistent with the renal damage levels determined by pathological analysis. Moreover, the high sensitivity of our KCK fluorescence imaging method even allowed the detection of the adaptive function of an unobstructed contralateral kidney (increased blood perfusion and enhanced clearance) when the obstructed kidney was severely damaged. These results clearly indicate that with the assistance of GS-AuNPs, noninvasive KCK fluorescence imaging can serve as an inexpensive and highly sensitive method for the noninvasive staging of kidney dysfunction in preclinical animal models, which is expected to greatly expedite the advancement of our fundamental understanding of kidney diseases.

[*] Dr. M. X. Yu, B. J. Du, X. H. Ning, Prof. Dr. J. Zheng
Department of Chemistry and Biochemistry
The University of Texas at Dallas
800 W. Campbell Rd., Richardson, TX 75080 (USA)
E-mail: jiezheng@utdallas.edu

Dr. J. C. Zhou, C. Authement, L. Gandee, Prof. Dr. P. Kapur, Prof. Dr. J. T. Hsieh, Prof. Dr. J. Zheng
Department of Urology
The University of Texas Southwestern Medical Center
5323 Harry Hines Blvd., Dallas, TX 75390 (USA)

Prof. Dr. P. Kapur
Department of Pathology
The University of Texas Southwestern Medical Center
5323 Harry Hines Blvd., Dallas, TX 75390 (USA)

Supporting information for this article is available on the WWW under http://dx.doi.org/10.1002/anie.201511148.

Near-infrared-emitting GS-AuNPs were synthesized with an approach that we had reported previously.[8] The core size and the hydrodynamic diameter of the GS-AuNPs were 2.5 ± 0.3 nm and 3.3 ± 0.4 nm, respectively.[8] As the hydrodynamic diameter of the GS-AuNPs in a native physiological environment is well below the kidney filtration threshold (6–8 nm), the NPs can be cleared out of the body through the kidneys with an efficiency comparable to those of clinically used small-molecule-based contrast agents.[9] Unlike near-infrared lipophilic organic fluorophores, which severely accumulate in the background tissues, the zwitterionic GS-AuNPs have extremely low accumulation in the background tissues;[6] therefore, the KCK of GS-AuNPs can be noninvasively and accurately monitored by in vivo fluorescence imaging.[6]

To investigate whether noninvasive KCK fluorescence imaging with renal-clearable GS-AuNPs can report on kidney dysfunction, we used a UUO mouse model, which was generated by complete ligation of the left ureter of the mouse while the right ureter was kept intact (Figure 1 A). For the sham-operated group, the left ureters were exposed but not ligated. At 7–9 days post-operation, characteristic structural changes of the kidney caused by the obstruction were confirmed by an ex vivo study (Figure 1 A). However, the UUO mice and the sham-operated control group showed no significant differences in blood urea nitrogen and serum creatinine; these are the most common biomarkers for renal function ($P > 0.05$, Table S1). This result is consistent with previous findings that blood urea nitrogen and serum creatinine are not good indicators of the renal function in a UUO model,[10] which is due to the presence of a well-functioning contralateral kidney.

With near-infrared-emitting GS-AuNPs as the contrast agent, we easily differentiated the UUO left kidney (UUO LK) from the unobstructed kidneys by noninvasive imaging and analysis of the TFICs (Figure 1 B–D and Figure S1, S2) whereas IRDye 800CW failed to do so because intensive skin background overwhelmed the real kidney signal (Figure S3). One minute after intravenous injection of the GS-AuNPs, the obstructed LK exhibited dramatically reduced fluorescence signals compared to the contralateral right kidney (RK) in UUO mice and the kidneys in the sham control group (Figure 1 B, Figure S1), corresponding to a remarkable decrease in the peak value (41.8 % on average) compared to that of the contralateral RK ($P < 0.05$, Figure 2 A and Table S2). Such a diminished accumulation of contrast agent in the UUO kidney indicates that the blood perfusion had been dramatically reduced upon obstruction, which is consistent with previous findings obtained by SPECT imaging of the KCK of UUO mice.[11] The reduced blood perfusion of the UUO LK resulted in an unequal functional status of the two kidneys in UUO mice. Under normal conditions, the two kidneys function equally well because for the sham control group, LK and RK contributed approximately 50 % to the relative renal function (% RRF = [peak value of LK or RK/(peak value of LK+peak value of RK)] × 100 %; Figure 2 B and Table S2). Upon obstruction of the LK, the % RRF value of the UUO LK decreased to 36.1 ± 2.4 % (Figure 2 B and Table S2), which is in agreement with its % RRF value obtained by SPECT imaging (34.6 ± 4.9 %).[5] Moreover,

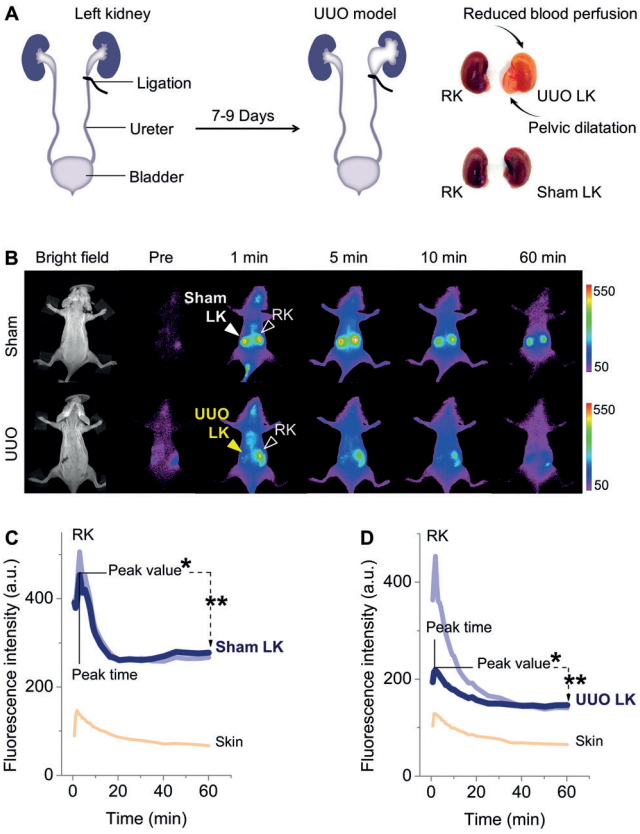

Figure 1. A) Unilateral ureteral obstruction (UUO) in mice was achieved by complete ligation of the left ureter while the right ureter was kept intact. In the sham-operated group, the left ureters were exposed but not ligated. B) Representative whole-body noninvasive fluorescence images of mice before and after intravenous injection of GS-AuNPs (Ex/Em filters: 710/830 nm). C, D) Time-fluorescence intensity curves (TFICs) of kidneys in the sham control group (C) and the UUO model (D). Four parameters were extracted from the kidney TFICs: peak value, peak time, *percentage of relative renal function (% RRF = [peak value of LK or RK/(peak value of LK+peak value of RK)] × 100 %), **clearance percentage at 60 min = [(peak value − intensity at 60 min)/peak value] × 100 %.

clearance of the NPs through the kidney (defined as the clearance percentage at 60 min = [(peak value − intensity at 60 min)/peak value] × 100 %; Figure 1 D) declined from 44.1 ± 6.6 % in sham LK to 31.3 ± 6.0 % in UUO LK (Figure 2 C and Table S2), which is also consistent with previous data obtained by SPECT imaging of a UUO model (the clearance percentage at 20 min dropped from ca. 79.1 % in the sham control group to ca. 13.7 % for UUO kidneys).[5] Furthermore, the differences in the peak times between the sham control group and the UUO models became statistically significant, which will be discussed below (Figure 2 D and Table S2).

Not only a kidney with declined function but also the stages of kidney dysfunction can be differentiated by noninvasive KCK fluorescence imaging. As shown in Figure 3 A, we observed three different patterns for the kidney TFICs of the UUO models, in addition to the kidney TFIC pattern of the sham control group (pattern (a); Movie S1). Aside from the TFIC pattern for the UUO kidney that is characterized by

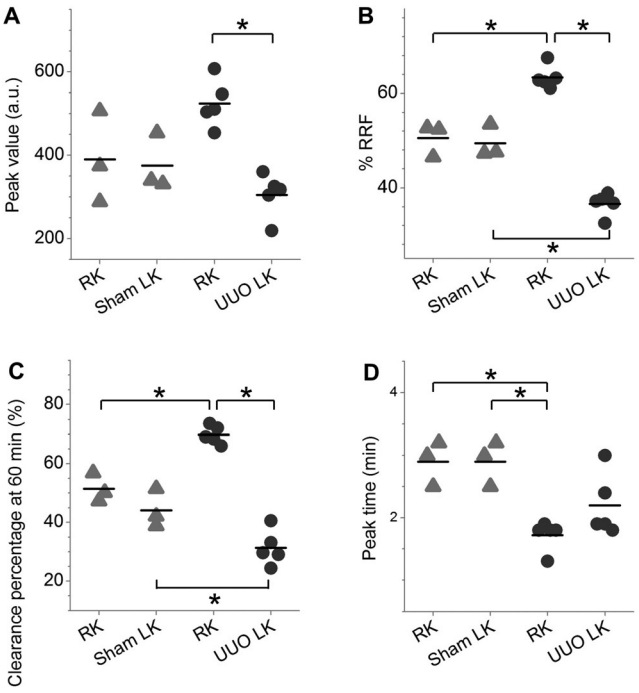

Figure 2. Statistical analysis of the four parameters extracted from the kidney TFICs of UUO mice and the sham control group. The parameters include A) the peak value, B) the relative renal function in % (% RRF), C) the clearance percentage at 60 min, and D) the peak time. Sham control group: triangle; UUO model: circle. $N=5$ for the UUO mice, $N=3$ for the sham control group. Mean values are given. $*P<0.05$.

a dramatic decrease in the peak value (pattern (b); Movie S2; see discussion above), we also observed another type of TFIC pattern with a relatively small reduction in peak value and prolonged retention in the kidney (pattern (c); Movie S3, Figure S4, Table S3). Pathological analysis of kidney tissue revealed that these two different TFIC patterns can be correlated with two degrees of renal damage: In kidneys with mild damage, the renal tubules showed mild to moderate atrophy and dilatation (total pathological score of 2; Table S4), whereas in kidneys with severe damage, renal tubular damage and cortical atrophy were much more pronounced (total pathological score of 4–6; Table S4, Figure 3B, left column). For the kidneys with mild damage, the peak value of the UUO LK was slightly reduced compared with the sham LK group but excretion through the kidney was slowed down (Figure 3A, pattern (c)). This mild-damage TFIC pattern was consistent with data obtained by SPECT imaging of UUO at an early stage (3 h post-operation, technetium-99 m mercaptoacetyltriglycine (^{99m}Tc-MAG3) as the contrast agent).[11] With the progression of renal damage to a severe level, the TFIC pattern changed to pattern (b): The peak value dramatically decreased, and the kidney TFIC resembled that of the blood background (skin TFIC; Figures 3A, 1D, and S2), implying that the kidney failure resulted from the severe injury.[12]

Aside from the staging of kidney dysfunction, in vivo fluorescence imaging was also sensitive enough to detect the adaptive function of contralateral RKs in the UUO mouse model. Even though no structural changes were observed in the contralateral RKs (Figure 3B, right column), a second decay phase was observed at 15–60 min for the kidney TIFCs of the UUO RK, following the initial decrease within the first 15 min (Figure 3A, pattern (d)), whereas for the sham group, the decrease in kidney intensity ended at 20 min post-injection (sham LK, Figure 3A, pattern (a); sham RK, Figure 1C and Figure S2). This two-phase decay contributed to a significant increase in the clearance of the GS-AuNPs

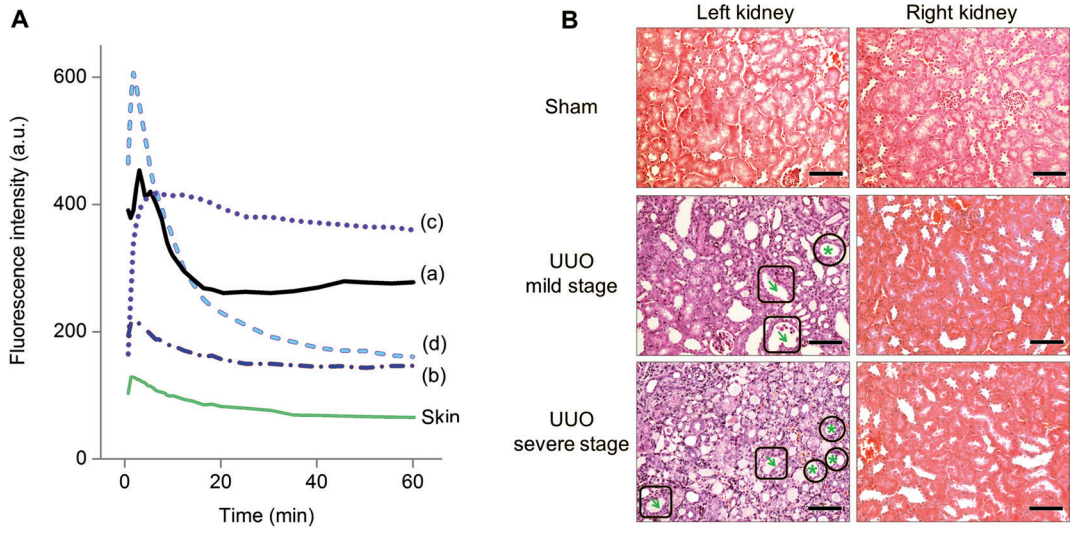

Figure 3. Correlation of the kidney TFIC patterns with the degree of renal damage. A) Representative TFICs of the sham LK (a), UUO LKs (b, c), and UUO RKs (d), corresponding to four statuses of kidney function: a) normal function, c) mild dysfunction, b) severe dysfunction, and d) adaptive function. The skin TFIC was obtained from the mouse that shows the pattern (b) of UUO LK. B) Pathologic analysis of kidneys of UUO mice and the sham control group (H&E stain, scale bar = 100 μm). Arrows in squares: tubular dilatation; stars in circles: tubular atrophy. The nucleus was stained in violet, and the cytoplasm was stained in pink. From the sham LK to the UUO LKs, the color change from pink to violet reflects a loss of cytoplasm, which is characteristic of cellular atrophy. The RKs were normal.

through the RKs owing to the injury of the LKs: The clearance percentage at 60 min increased from 51.5 ± 4.9 % in the sham control group to 69.8 ± 3.0 % in the UUO model ($P < 0.05$; Figure 2C and Table S2). The average peak value of the RK in UUO models with severe dysfunction was much higher than that in the sham control group (524.3 ± 56.9 vs. 389.9 ± 109.7; Figure 2A and Table S2), suggesting enhanced blood perfusion. The % RRF of the contralateral RK increased from the normal value of approximately 50 % to 63.4 ± 2.4 % in UUO mice ($P < 0.05$; Figure 2B and Table S2). The first peak appeared earlier than that of the sham RK (1.7 ± 0.2 min vs. 2.9 ± 0.4 min, $P < 0.05$; Figure 2D and Table S2), further indicating enhanced excretion of the GS-AuNPs through the healthy RKs of UUO mice.

In summary, in combination with GS-AuNPs, in vivo fluorescence imaging is sensitive enough to differentiate between kidneys with normal function, mild or severe dysfunction, and even adaptive function in UUO mice (Figure 4), which has not been possible with conventional markers such as blood urea nitrogen and serum creatinine. The high sensitivity is due to the high-contrast imaging of the KCK of renal-clearable near-infrared-emitting GS-AuNPs, which provides rich information on kidney function, including blood perfusion, relative functional status of the two kidneys, and the clearance capability.

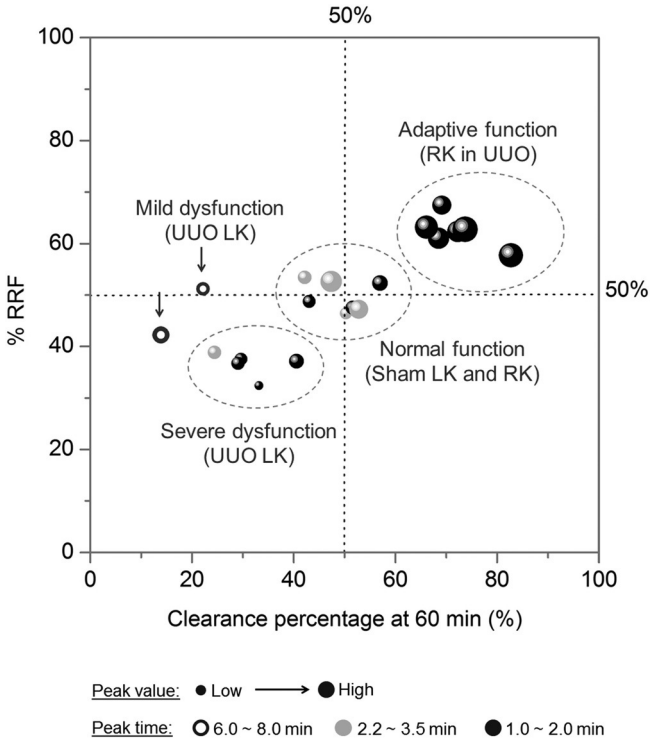

Figure 4. The four functional statuses of the kidney in the UUO model can be clearly differentiated by plotting the four parameters of the TFICs in one graph. X = clearance percentage at 60 min, Y = % RRF. The bubble size corresponds to the peak value, and the bubble shading to the peak time (black: 1.0–2.0 min; gray: 2.2–3.5 min; hollow circle: 6.0–8.0 min). Data were obtained from 20 kidneys in 10 mice and presented in Table S2 and S3. $N = 7$ for the UUO model; $N = 3$ for the sham control group.

It should also be noted that the GS-AuNP TFICs of the UUO kidneys were not completely identical to the time–activity curves obtained by SPECT kidney imaging with ^{99m}Tc-MAG3 as the contrast agent: Once the peak value had been reached, a decay phase was observed in the TIFCs determined with the GS-AuNPs (Figure 3A, pattern (b); Figure S2) whereas the signal was maintained at a constant level in the ^{99m}Tc-MAG3 based activity curves.[11] This difference implies that the renal excretion mechanism for the GS-AuNPs is likely to be different from that of ^{99m}Tc-MAG3 (predominantly excreted by tubular secretion). Fluorescence microscopy imaging of kidney sections revealed that the GS-AuNPs were mainly distributed in the glomeruli at 5 min post-injection (Figure S5), suggesting that glomerular filtration was likely a major clearance route for the GS-AuNPs. However, how exactly the GS-AuNPs are excreted through the kidney needs further investigation. Moreover, pathological analysis of the kidneys in the sham mice revealed no structural alteration after intravenous injection of GS-AuNPs (Figure 3B), suggesting that the GS-AuNPs are of low renal toxicity. The results presented in this study thus suggest that in vivo fluorescence imaging could serve as a powerful and sensitive preclinical method for determining kidney function and advancing our fundamental understanding of kidney disease progression.

Acknowledgements

This study was supported by the NIH (1R01DK103363), CPRIT (RP140544), and a start-up fund from the University of Texas at Dallas. We thank Prof. Chou-Long Huang, Prof. Chandra Mohan, and Prof. Yong Du for insightful discussions.

Keywords: fluorescence imaging · imaging agents · kidney disease · kidney dysfunction · nanoparticles

How to cite: *Angew. Chem. Int. Ed.* **2016**, *55*, 2787–2791
Angew. Chem. **2016**, *128*, 2837–2841

[1] a) R. A. Star, *Kidney Int.* **1998**, *54*, 1817–1831; b) L. S. Chawla, P. W. Eggers, R. A. Star, P. L. Kimmel, *N. Engl. J. Med.* **2014**, *371*, 58–66.
[2] a) A. T. Taylor, *J. Nucl. Med.* **2014**, *55*, 608–615; b) N. Grenier, F. Basseau, M. Ries, B. Tyndal, R. Jones, C. Moonen, *Abdom. Imaging* **2003**, *28*, 164–175; c) J. D. Krier, E. L. Ritman, Z. Bajzer, J. C. Romero, A. Lerman, L. O. Lerman, *Am. J. Physiol. Renal. Physiol.* **2001**, *281*, F630–F638.
[3] R. Weissleder, M. J. Pittet, *Nature* **2008**, *452*, 580–589.
[4] a) B. A. Kairdolf, A. M. Smith, T. H. Stokes, M. D. Wang, A. N. Young, S. M. Nie, *Annu. Rev. Anal. Chem.* **2013**, *6*, 143–162; b) H. Hyun, E. A. Owens, H. Wada, A. Levitz, G. Park, M. H. Park, J. V. Frangioni, M. Henary, H. S. Choi, *Angew. Chem. Int. Ed.* **2015**, *54*, 8648–8652; *Angew. Chem.* **2015**, *127*, 8772–8776; c) S. D. Perrault, W. C. W. Chan, *Proc. Natl. Acad. Sci. USA* **2010**, *107*, 11194–11199.
[5] F. J. Penna, J. S. Chow, B. J. Minnillo, C. C. Passerotti, C. E. Barnewolt, S. T. Treves, F. H. Fahey, P. S. Dunning, D. A. Freilich, A. B. Retik, H. T. Nguyen, *J. Urol.* **2011**, *185*, 2405–2413.
[6] M. X. Yu, J. B. Liu, X. H. Ning, J. Zheng, *Angew. Chem. Int. Ed.* **2015**, *54*, 15434–15438; *Angew. Chem.* **2015**, *127*, 15654–15658.

[7] a) S. Decramer, S. Wittke, H. Mischak, P. Zurbig, M. Walden, F. Bouissou, J. L. Bascands, J. P. Schanstra, *Nat. Med.* **2006**, *12*, 398 – 400; b) I. Ulman, V. R. Jayanthi, S. A. Koff, *J. Urol.* **2000**, *164*, 1101 – 1105.
[8] J. B. Liu, M. X. Yu, C. Zhou, S. Y. Yang, X. H. Ning, J. Zheng, *J. Am. Chem. Soc.* **2013**, *135*, 4978 – 4981.
[9] a) C. Zhou, M. Long, Y. P. Qin, X. K. Sun, J. Zheng, *Angew. Chem. Int. Ed.* **2011**, *50*, 3168 – 3172; *Angew. Chem.* **2011**, *123*, 3226 – 3230; b) C. Zhou, G. Y. Hao, P. Thomas, J. B. Liu, M. X. Yu, S. S. Sun, O. K. Oz, X. K. Sun, J. Zheng, *Angew. Chem. Int. Ed.* **2012**, *51*, 10118 – 10122; *Angew. Chem.* **2012**, *124*, 10265 – 10269; c) M. X. Yu, J. Zheng, *ACS Nano* **2015**, *9*, 6655 – 6674.
[10] S. Chung, H. Yoon, S. Kim, S. Kim, E. Koh, Y. Hong, C. Park, Y. Chang, S. Shin, *Nutr. Metab.* **2014**, *11*, 2.
[11] M. N. Tantawy, R. Jiang, F. Wang, K. Takahashi, T. E. Peterson, D. Zemel, C.-M. Hao, H. Fujita, R. C. Harris, C. C. Quarles, T. Takahashi, *BMC Nephrol.* **2012**, *13*, 168.
[12] E. Fommei, S. Ghione, A. J. W. Hilson, L. Mezzasalma, H. Y. Oei, A. Piepsz, D. Volterrani, *Eur. J. Nucl. Med.* **1993**, *20*, 617 – 623.

Received: December 1, 2015
Published online: January 22, 2016

